Only Subtle Protein Conformational Adaptations Are Required for Ligand Binding to Thyroid Hormone Receptors: Simulations Using a Novel Multipoint Steered Molecular Dynamics Approach

Leandro Martínez,[†,§] Igor Polikarpov,[‡] and Munir S. Skaf*[,†]

Institute of Chemistry, State University of Campinas-UNICAMP, P.O. Box 6154, Campinas, SP, 13084-862, Brazil, and Instituto de Física de São Carlos, Universidade de São Paulo, São Carlos, SP, 13560-970, Brazil

Received: April 18, 2008; Revised Manuscript Received: June 19, 2008

Thyroid hormone receptors (TR) are hormone-dependent transcription regulators that play a major role in human health, development, and metabolic functions. The thyroid hormone resistance syndrome, diabetes, obesity, and some types of cancer are just a few examples of important diseases that are related to TR malfunctioning, particularly impaired hormone binding. Ligand binding to and dissociation from the receptor ultimately control gene transcription and, thus, detailed knowledge of binding and release mechanisms are fundamental for the comprehension of the receptor's biological function and development of pharmaceuticals. In this work, we present the first computational study of ligand entry into the ligand binding domain (LBD) of a nuclear receptor. We report molecular dynamics simulations of ligand binding to TRs using a generalization of the steered molecular dynamics technique designed to perform single-molecule pulling simulations along arbitrarily nonlinear driving pathways. We show that only gentle protein movements and conformational adaptations are required for ligand entry into the LBDs and that the magnitude of the forces applied to assist ligand binding are of the order of the forces involved in ligand dissociation. Our simulations suggest an alternative view for the mechanisms ligand binding and dissociation of ligands from nuclear receptors in which ligands can simply diffuse through the protein surface to reach proper positioning within the binding pocket. The proposed picture indicates that the large-amplitude protein motions suggested by the apo- and holo-RXRα crystallographic structures are not required, reconciling conformational changes of LBDs required for ligand entry with other nuclear receptors apo-structures that resemble the ligand-bound LBDs.

1. Introduction

Nuclear hormone receptors (NR) consist one of the largest families of ligand-inducible transcription factors and play key roles in cell differentiation, homeostasis, and a wide range of physiological functions. NRs are, therefore, important therapeutic targets for a variety of human diseases including, cancer, diabetes and other metabolic disorders. Several lipophilic organic molecules, including estrogenic contraceptives, corticoids and glucocorticoids, androgen hormones, retinoids, fatty acids, and the thyroidal hormones, are involved in the control of developmental and metabolic processes by binding into NR.[1,2] Ligand binding induces conformational changes in the NRs that promote corepressor dissociation and coactivator recruitment and trigger the transcription of specifically targeted genes.

NRs are modular proteins consisting of three domains: an N-terminal domain, which contains an activation factor (AF-1), a DNA binding domain (DBD), which recognizes specific sequences of nucleotides and, thus, specifies the genes to be regulated, and a C-terminal domain, which is connected by a mobile hinge to the DBD and is responsible for the largest set of functions. The most notable functional role of the C-terminal domain is ligand binding and recognition. Therefore, it is known as the ligand binding domain (LBD).[3] The LBD also contains dimerization surfaces, an activation factor (AF-2), and the interfaces for the recognition of coregulator proteins.[4] It is generally accepted that ligand binding-induced rearrangements of the LBD C-terminal helix (helix 12) promote the dissociation of a corepressor protein and forms the binding surface for a coactivator, as shown in Figure 1a.[5] Once the coactivator is bound, gene transcription is initiated. Therefore, the fundamental process underlying the control of NR-regulated gene transcription is the process of ligand binding and dissociation.

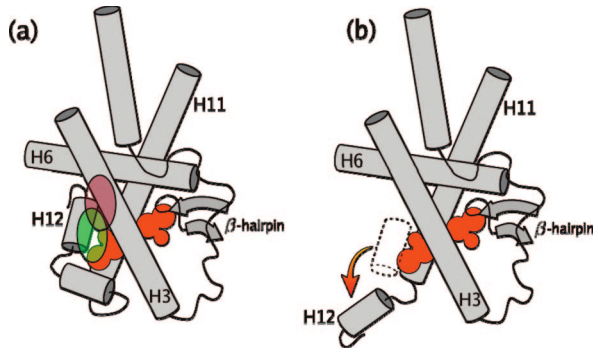

Figure 1. (a) Schematic representation of the coactivator (green) and corepressor (red) interaction surfaces, which depend on the position of the H12. (b) Movement of the C-terminal helix (H12) suggested by holo- and apo-RAR structures that would allow for ligand (orange) entry and exit the binding pocket in the "mousetrap" model.

Unlike the active sites of enzymes, which are typically clefts on the external surface of the protein, the binding site of NRs

* Corresponding author. E-mail: skaf@iqm.unicamp.br.
† State University of Campinas-UNICAMP.
‡ Universidade de São Paulo.
§ Present address: Structural Bioinformatics Unit, Institute Pasteur, Paris, France.

10.1021/jp803403c CCC: $40.75
Published on Web 08/06/2008

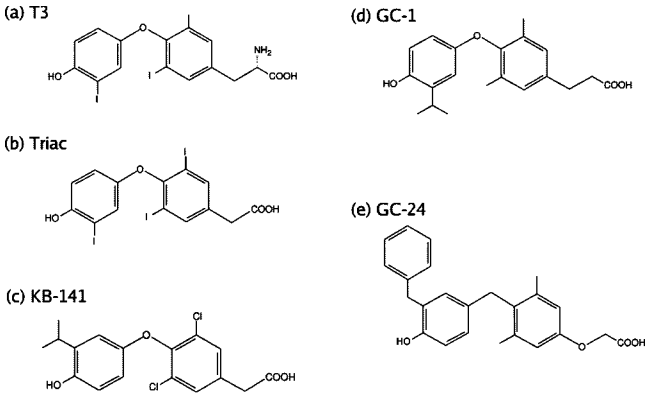

Figure 2. TR ligands: natural ligands (a) T3 and (b) Triac. Synthetic β-selective ligands (c) KB141, (d) GC1, and (e) GC24.

is buried in the hydrophobic core of the receptor, presenting no obvious ligand entry or exit routes. It is widely believed that significant LBD structural rearrangements must accompany ligand binding into and release from the NR binding pocket.[6,7] However, the molecular mechanisms associated with these processes are yet poorly understood. We and others have used molecular dynamics (MD) simulations to investigate mechanisms of ligand dissociation from various NRs, and these studies have provided valuable insights into the unbinding processes.[8−14] In contrast, how ligands enter the binding pocket remains essentially unexplored. This in part can be explained by the lack of unliganded structures for most of nuclear receptors, but mostly resides in the absence of suitable computational techniques capable of handling the complexity of ligand entry into the deeply buried binding pocket of NRs.

In this paper, we present a generalization of the steered molecular dynamics (SMD) simulation method[15] that can perform single molecule pulling simulations along an arbitrarily shaped path and apply the technique to assist binding of natural and synthetic ligands of the thyroid hormone nuclear receptor (TR). As further described, the method requires a set of user-supplied restraining points that grossly specifies the desired nonlinear pulling pathway and, conveniently, yields a continuous time profile of the applied force modulus, which is an important feature for analysis of SMD trajectories.[15] Using this multipoint steered molecular dynamics (MP-SMD) approach, we have been able to simulate the complex process of ligand entry into NRs for the first time. We report here ligand binding of the natural thyroidal hormones T3 and Triac and the thyromimetics GC1, GC24, and KB141 (Figure 2) into the LBDs of the TRα and TRβ isoforms, totaling 74 independent MP-SMD simulations. We have chosen TR for the present study not only because of its biochemical and medical importance but also because it constitutes one of the most studied cases of ligand dissociation from NRs using MD simulations.

In what follows, we present background information on NR LBD dynamics and summarize the main aspects regarding ligand dissociation pathways for TR and other nuclear receptors identified previously by MD simulations. In section 3, we describe our multipoint generalization of the SMD technique and provide simulation details and structural models used. Results and Discussion are presented in section 4, where we analyze global features of the simulations and suggest the nature of the protein movements required for ligand binding. Summary and concluding remarks are in section 5.

2. Nuclear Receptors Background

A. LBD Dynamics and Ligand Dissociation. There are several studies on the dynamical aspects of the LBDs of NRs.

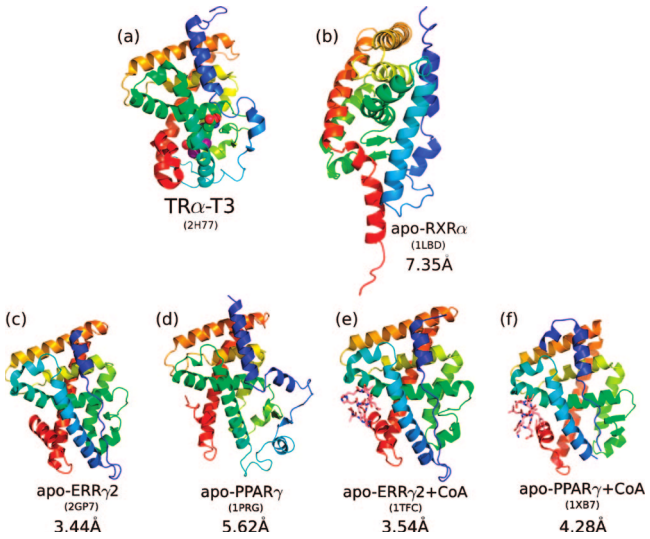

Figure 3. Comparison between the ligand binding domains of holo-thyroid hormone receptors (a) and apo-LBDs of other receptors (b−f). The apo-RXRα structure (b) shows the open H12 conformation (red), while apo-estrogen (ERR) and apo-peroxisome proliferator activated (PPAR) receptors reveal closed H12 conformations in the absence (c, d) and or in the presence (e, f) of coactivator peptides. The RMSDs of each apo structure relative to the holo-TRα LBD and PDB ids are indicated.

Most of them seek for functional roles of the helix 12 (H12) and have been largely motivated by correlations between the structures of the ligand-bound (holo) and ligand-free (apo) retinoic acid receptors (RAR) obtained in the mid 1990s.[7,16,17] These structures were one of the first LBD structures to be determined experimentally and suggested a mechanism for ligand entry and exit the binding pocket. Comparison between the apo- and holo-RAR structures reveals that the most notable difference is the unpacking of the H12 away from the body of the receptor in the apo structure,[6,7] as opposed to its "closed lid", active conformation in the presence of the ligand. This movement of the C-terminal helix (represented in Figure 1b) opens the binding cavity and could allow for ligand binding or dissociation. This mechanism of receptor-regulated ligand binding is known as the "mousetrap" model.[6,16] Another liganded structure in which H12 is displaced from the body of the LBD has been reported for the human ERα LBD bound to estradiol.[18,19] However, as the authors pointed out, the H12 conformation is attributed to a peculiar crystal packing effect. Indeed, Celik et al.[20] have recently observed the systematic closing of H12 in MD simulations of this structure in the absence of the ligand. Other studies were further performed seeking for correlations between H12 and ligand dynamics. For instance, it was found that binding of estrogen agonists to the estrogen receptor (ER) protected H12 from trypsin cleavage, whereas antagonist binding has a much smaller protective effect.[21] Moreover, studies on several NRs support the view that coactivator binding requires the active H12 positioning similar to that observed for the holo-RAR (cf. Figure 1a),[22−24] but some ER antagonists, like tamoxifen, for instance, induce incorrect folding of H12 on the body of the receptor.[25]

The movements of H12 seem to be less prominent than was originally suggested by RAR structures. Structures of other unliganded LBDs, such as the apo structures of PPARγ,[23] ERRγ2,[26] and the orphan receptors NGFI-B[27] and DHR38,[28] are more similar to the holo-RAR structure than to the ligand-free RAR, as shown in Figure 3. Even structures of the coactivator bound (but ligand free) PPARγ and ERRγ2 reveal

closed H12 conformations (Figure 3d−e). Moreover, several receptors have some constitutive activity (activity in the absence of ligand), thus showing that H12 can be found in the active conformation even in the absence of the ligand.[29,30] Therefore, the canonic image of two structures, one related to the apo and other to the holo receptor states, remains controversial. Notwithstanding, spectroscopic studies show that binding of cofactors and several distinct mutations perturb H12 dynamics and provide compelling evidence that the dynamical conformational equilibrium of H12 is influenced by ligand binding.[20,21,31−34] It is not unlikely, however, that such equilibrium would involve mostly local conformational variations, instead of a complete detachment of H12 from the core of the LBD.

MD simulations have contributed significantly to the understanding of the molecular mechanisms of ligand dissociation. MD studies of ligand unbinding have been reported for RARs,[8−10] TRs,[11,12] and PPARγ.[13] Very recently, simulation studies have been reported for the dissociation of 17β-estradiol and a tissue selective ER modulator, raloxifene, from the monomeric and dimeric forms of the ER LBD.[14] The first two pioneer studies[8,9] were performed for the dissociation of the retinoic acid from its receptor RAR and used two different techniques: locally enhanced sampling molecular dynamics (LES),[8,35] which allows for the identification of probable dissociation mechanisms, and steered molecular dynamics (SMD),[9,15] in which an external force is applied along a previously selected direction to assist ligand unbinding. Simulations using LES show retinoic acid dissociation from the receptor body only through the displacement of H12, reminiscent of the mousetrap model.[8] The SMD simulations on the same RAR structure performed by Schulten and collaborators,[9] on the other hand, suggested that other escape routes could exist. In particular, it was suggested that the ligand could leave the receptor through the expansion of a small surface aperture near the H1−H3 loop and β-hairpin, a highly mobile region of the LBD. More recently, results from random expulsion molecular dynamics simulations on RAR provided further support to this alternative pathway for ligand dissociation.[10] In our laboratory, we have performed independent systematic investigations of the unbinding pathways of several ligands from TR[11,12] and ER,[14] in which multiple dissociation routes were identified and, for the case of TR, their relative importance assessed.[12] A more detailed description of the multiple dissociation pathways of ligands from TR obtained from these studies is summarized below.

B. TR and Dissociation Pathways. Thyroid hormone receptors (TRs) are involved in the control of the basal metabolism and cellular differentiation and are related to several human diseases, such as hyper- and hypothyroidism, diabetes, obesity, osteoporosis, and some cancers.[36−38] In particular, hyper- and hypothyroidism are usually genetic diseases caused by mutations in the LBD of TRs leading to impaired hormone binding.[39] Hypothyroidism can be treated by the administration of the natural hormone 3,5,3′-triiodo-L-thyronine (T3). However, thyroid hormone replacement therapy may have important side effects, such as gain or loss of weight, loss of bone and muscle mass, heart malfunction (tachycardia, for example), and even bipolarity.[40] The effects of T3 on heart tissues are the major drawback of T3 use in the treatment of obesity. Interestingly, these effects are caused by the activity of the hormone in different receptor isoforms.

There are basically two TR isoforms, TRα and TRβ. TRα is mostly responsible for thyroid hormone physiological effects in heart tissues, whereas TRβ is found predominantly in liver and kidneys. TRβ is thus a promising target for the development of drugs for obesity and hypothyroidism therapies.[41] Its high concentration in the liver links TRβ to the rates of fat and cholesterol metabolisms, but not to the effects that the natural hormones induce in the heart.[42] As a consequence, current treatments of these diseases may be performed using the natural TRβ-selective T3 metabolite known as Triac. However, Triac still has high affinity for TRα and undesirable side effects over the heart must be carefully monitored. Other synthetic ligands showing higher β-selectivity have been developed.[43−50] These ligands, including GC1, have been demonstrated to induce body fat loss and reduce serum cholesterol levels in rats, without promoting deleterious side effects in the heart.[42,43] Unfortunately, as yet there is still no such ligand approved for human administration. Some of these ligands, which were used in the present study, are represented in Figure 2.

Insights into the mechanisms of ligand binding and dissociation have been obtained for TRs from similarity to other receptors, structural studies with synthetic ligands, and from MD simulations. The structure of the LBD of TRs is similar to the structure of the RAR and other NRs and is composed by 12 helices and two small β-sheets.[51] The crystallographic structure of T3 bound TRβ suggested that the region of the β-hairpin, displaying large temperature B-factors, could be a pathway for ligand entry.[51] The similarity between liganded TR and RAR LBD structures suggests that H12 dynamics could also play an important role in ligand binding and dissociation in TR. However, experimental evidence relating ligand and TR dynamics is still lacking. Recently, we performed extensive MD simulations of ligand dissociation from TRs that allowed us to map the mobility of the LBD and sample configurational space for putative dissociation routes,[11] and to assess likelihood of dissociation mechanisms and their corresponding molecular basis.[12] Our studies showed that TR could harbor multiple ligand escape pathways.[11] Three important dissociation mechanisms were found. The first mechanism (Path I) involves the displacement of the H12 from H3 (although not necessarily a full detachment of the helix from the LBD), and resembles the mousetrap mechanism for the dissociation of the retinoic acid from the RAR receptor.[8] Another dissociation route encountered in the simulations, Path II, involves the separation between helices 8 and 11 and the mobile Ω-loop. This pathway was not previously suspected in spite of its involving one of the most mobile loops of the LBD.[51] Recent simulations support the existence of such path for ligand dissociation for estrogen receptors.[14] In the third dissociation pathway, the ligand leaves the receptor through the hydrophilic cavity formed by rearrangements in the β-hairpin and the loop between H1 and H2. Subsequent SMD simulations have suggested that Path III is the likeliest ligand dissociation pathway in TR.[12] Our simulations indicated that dissociation through this region is favored because the hydrophilic contacts between ligand and LBD are substituted by interactions between the ligand polar head and external water molecules with no appreciable energetic cost.[12]

3. Multipoint SMD and Simulation Details

The study of ligand binding events into the core of nuclear receptors' LBDs requires a generalization of the SMD technique used for simulating ligand−NR dissociation in which only constant pulling directions are allowed for.[9,12,15] This is because the mechanisms of binding start from a highly entropic ill-defined initial ligand position and must end with the ligand adopting a precise orientation in the binding pocket, therefore requiring multiple (usually a few) bending points at which the

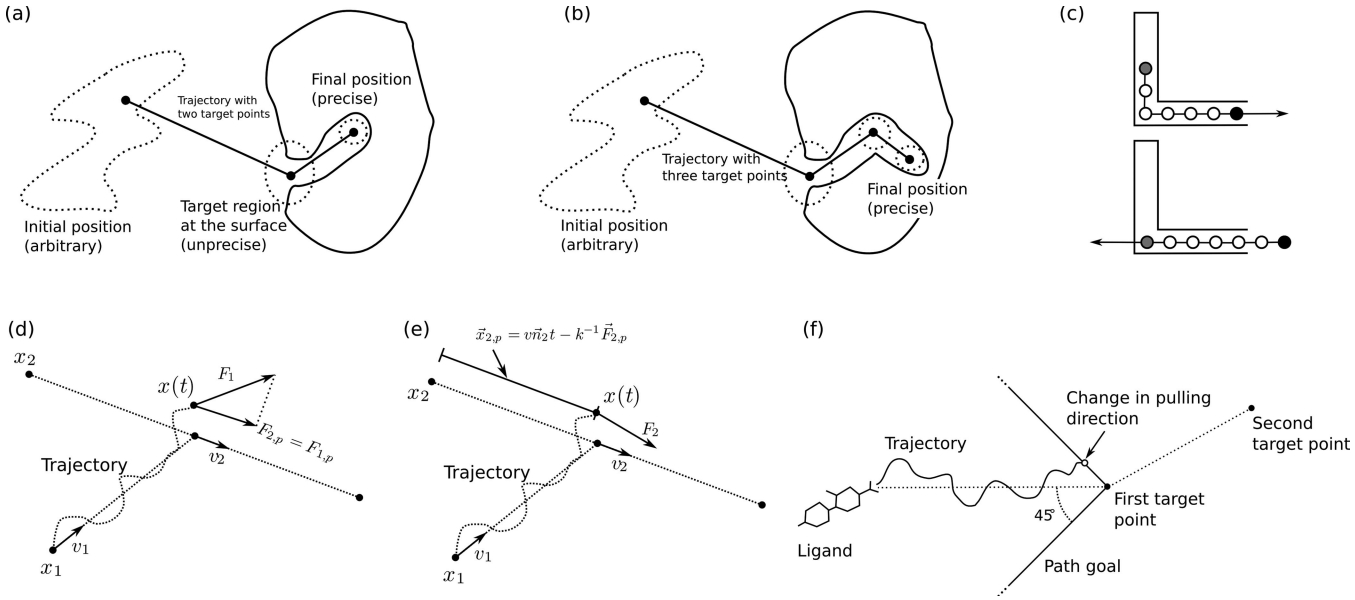

Figure 4. Need for a generalized SMD approach. (a) Even the simplest binding mechanism requires a curved trajectory for the ligand to reach the correct region at the protein surface. (b) More complex structures require more complex trajectories, defined by many target points. (c) The pearl-necklace/tube toy model illustrates how equivalent binding and dissociation trajectories may require different SMD approaches. (d) For applying the generalized SMD approach, the parallel component of the force along the new direction, $\mathbf{F}_{1,p}$, is conserved. (e) A new reference position, $\mathbf{x}_2$, is defined such that the parallel component of the force is preserved. (f) To define when a trajectory step has been fulfilled, we define a cone with the vertex at the target point. The trajectory step is fulfilled when the pulled site crosses the cone's surface.

direction of the pulling force is changed, as illustrated in Figure 4, a and b. Driving ligand binding into the LBD at constant pulling direction, in contrast, involves unreasonably large protein structural rearrangements and physically insensible energy barriers and often fails to reach proper ligand binding mode within the protein pocket. The unbinding trajectories investigated using conventional SMD simulations are qualitatively similar to the trajectories employed here. Ligand dissociation from NR LBD is more easily generated with conventional SMD because each unbinding path is promoted by the pulling of a ligand atom close to the surface of the protein. The rest of the hormone simply follows the pulled atom and the inner parts of the ligand follow nonlinear trajectories in spite of the fact that the tagged atom is pulled along a rectilinear driving path. The same cannot be achieved for binding simulations. In this case, the pulled atom must be the one crossing the binding pocket and, therefore, turns must be induced. A simplified picture illustrating the need for intermediate restraining points is that of pearl necklace inside a curved tube (Figure 4c). Dissociation can be easily achieved by pulling a bead located near the tube's edge: the rest of the necklace will naturally glide through the curved trajectory even if the pulling direction is constant. Association, instead, requires a pulling force that changes direction.

A. MP-SMD: A Generalization for Nonlinear Trajectories. As generally described in the literature, the celebrated steered molecular dynamics approach is devised for linear driving paths.[15] The SMD approach consists of applying an external force to an atom, or group of atoms in the simulation, in order to drive its motion according to the equation

$$\mathbf{F} = k[\mathbf{v}t - \Delta\mathbf{x}(t)] \quad (1)$$

where $\mathbf{v}$ is a constant vector that points to a fixed point in space (restraining point) and defines the pulling direction, $\Delta\mathbf{x}(t)$ is the tagged group displacement relative to its initial position, t is the simulation time, and k is a constant that specifies the stiffness of the applied harmonic restraining force. This functional form is interesting because the time history of the applied force reflects the resistance exerted by the environment on the tagged group and provides information about barriers and related molecular processes along the pulling.[9,15]

Variations of the SMD method have been developed to study problems for which the unidirectional pulling approach is unsuitable. For example, Schulten and co-workers applied a torque to the Rieske subunit of cytochrome bc(1) complex to study a molecular mechanism in which a rotation is involved.[52] More complex driving paths are necessary to study ligand binding into the hydrophobic pocket of NRs and probably other ligand−protein systems.[53,54] The NAMD[55,56] and VMD[57] packages, on the other hand, allow the user to interactively change the pulling direction, but this is not practical in many situations unless powerful interfacing and computational resources are available.[58]

For any given driving path, the key feature one would like to preserve in a single-molecule pulling simulation is the environment modulation of the applied force in terms of the elapsed simulation time and displacement relative to the initial position; that is, one would like to generate a force profile that portrays the environment resistance to the pulling.[15] Evidently, eq 1 is unsuitable for a nonlinear driving path (in a closed path, for instance, $\Delta\mathbf{x}$ would vanish at the end). The fundamental idea behind our generalized implementation of SMD is very simple and consists in representing an arbitrary curvilinear pulling path by a discrete set of piecewise linear segments to which the usual SMD method, eq 1, is independently applied. The key feature is that the multiple connecting points define new references or "initial positions" for calculating atomic displacements $\Delta\mathbf{x}$, as described below.

Let us consider a path consisting of a series of connected linear segments and that to each segment conventional SMD force is applied with same k and $|\mathbf{v}|$ values, according to eq 1. Suppose the pulling force has been applied for the first segment (unit direction $\mathbf{n}_1$) and the restrained atom has reached its first target point, in such a way that the force must now be reoriented

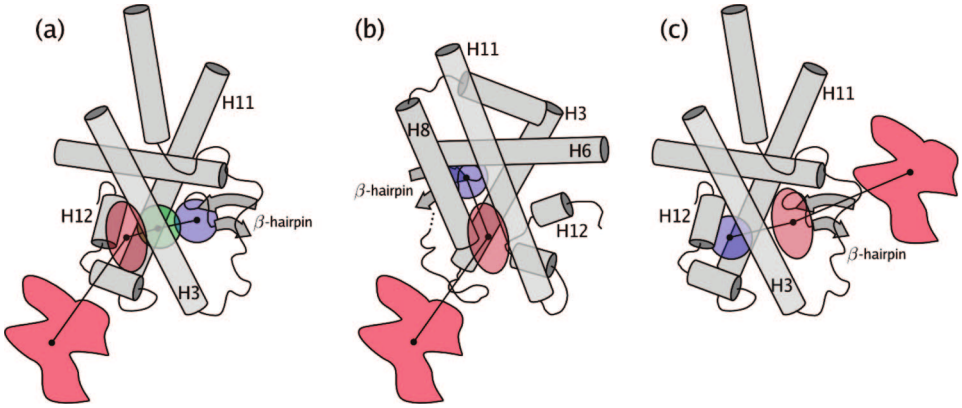

Figure 5. Binding trajectories based on previous unbinding simulations. (a) Path I: A four-point path which involves the displacement of the H12. (b) Path II: Three-point trajectory in which the ligand enters the binding pocket within the helices 8 and 11. (c) Path III: Binding occurs through the mobile and hydrophilic region around the β-hairpin, and the trajectory is represented also by three points.

to point to the second target (direction $\mathbf{n}_2$), as shown in Figure 4d. At this instant, the applied force is given by

$$\mathbf{F}_1 = k[v\mathbf{n}_1 t - (\mathbf{x}(t) - \mathbf{x}_1)] \quad (2)$$

where $\mathbf{x}(t)$ and $\mathbf{x}_1$ are the current and initial positions of the pulled site, respectively. When the pulling direction is to be changed, it is reasonable to preserve the component of the force $\mathbf{F}_1$ along the new direction. This is accomplished by projecting $\mathbf{F}_1$ along $\mathbf{n}_2$ to obtain the parallel component $\mathbf{F}_{2,p}$ of the new force along $\mathbf{n}_2$ at time t:

$$\mathbf{F}_{2,p} = \langle \mathbf{F}_1 | \mathbf{n}_2 \rangle \mathbf{n}_2 \quad (3)$$

From this point on, the original initial position $\mathbf{x}_1$ can no longer be used to compute displacements in an SMD pulling (eq 1) along segment 2 without introducing undesirable effects in the modulation of the applied force. To circumvent this drawback, we redefine the "initial point" of the trajectory, consistently with the new pulling direction, such that the force profile preserves information about the barriers involved. Given $\mathbf{F}_{2,p}$ from eq 3, we compute a new "parallel displacement" vector, $\mathbf{x}_{2,p}$, according to

$$\mathbf{x}_{2,p} = v\mathbf{n}_2 t - k^{-1}\mathbf{F}_{2,p} \quad (4)$$

$\mathbf{x}_{2,p}$ corresponds to the displacement that would be associated to a force $\mathbf{F}_{2,p}$ in a hypothetical situation of pulling along direction $\mathbf{n}_2$ from the start of the simulation ($t = 0$) (Figure 4e). The component of the new displacement vector orthogonal to $\mathbf{n}_2$, $\mathbf{x}_{2,o}$, corresponds simply to the distance between the line that defines the new path and the current position of the pulled site. This provides the means for defining the new displacement vector $\mathbf{x}_2$:

$$\mathbf{x}_2 = \mathbf{x}(t) - (\mathbf{x}_{2,p} + \mathbf{x}_{2,o}) \quad (5)$$

The pulling force for segment 2, from the moment the force switches direction up to end of this trajectory step, is computed from eq 1 by taking $\Delta\mathbf{x} = \mathbf{x}(t) - \mathbf{x}_2$.

Therefore, what we do for generalizing the SMD force for an arbitrary trajectory is to define a time-dependent reference position that substitutes the "initial coordinates" of the pulled site. This time-dependent reference is computed as to preserve the force component parallel to the new pulling direction. The force computed in this way preserves modulation in terms of the time and displacement, with displacement being redefined at each intermediate restraining point as described. For a linear trajectory, this procedure results identical to the usual SMD approach, since $\mathbf{n}_1 = \mathbf{n}_2$, and, therefore, $\mathbf{F}_{2,p} = \mathbf{F}_{1,p}$ from eq 2. For smooth and continuous trajectories, for which $\mathbf{n}_1 \sim \mathbf{n}_2$ the force will be also continuous and smooth. Driving paths of any complexity can be simulated using this protocol by introducing a sufficient number of intermediate restraining points.

A technical detail for the definition of the "end" a given path segment must be given. One cannot ensure that the pulled site will reach the target point connecting consecutive segments with an arbitrary precision because of the thermal fluctuations of the pulled group. Therefore, we define that a trajectory step ends when the pulled site crosses the surface of a cone with a vertex at the target point, as shown in Figure 4f. This event will necessarily occur and, therefore, is a satisfactory criterion. In practice, we observed that the restrained atom generally passes in the immediate vicinity of the target point, such that other criteria (e.g., minimum given distance between actual position and target point) could be used with similar results.

B. Definition of Binding Pathways for TR. We consider ligand binding through the three different regions of the TR LBD that have been previously identified as possible dissociation routes, namely, Paths I−III,[11,12] already described. These pathways were obtained from locally enhanced sampling simulations of ligand dissociation,[11,35] which do not require any a priori assumption from the investigator. Other strategies could be used for different systems. For binding through region I, a three-step driving path was devised (Figure 5a) to achieve correct ligand positioning in the binding pocket, whereas successful binding through regions II and III required only a single change in force direction, as shown in Figure 5, b and c. The MP-SMD algorithm was implemented in such a way that the driving paths could be defined in terms of the protein atom coordinates. For example, the first change in the pulling direction in a trajectory based on Path I was performed when the ligand carboxylate carbon reached, for example, the average position of atoms Thr223-Cα of H3 and atom Phe401-Cα of H12 (residue numbers refer to the TRα sequence), as represented in Figure 5a. For each simulation, different Cα in the vicinity of these atoms were chosen in order to improve sampling. The final target points for Paths I and II were specified by a distance of about 2 Å between the carboxylate of the ligand and one of the arginines of the polar head of the binding pocket (either Arg228 or Arg262 or Arg266 depending on which residue was closer to the ligand in the native structure). For Path III, the final point of the trajectory was defined by the distance between the phenolic oxygen of the ligands and the Histidine 381/435 which form a hydrogen bond in the crystallographic structures.[51] Further details is provided in Figure S1 of Supporting Informa-

tion. It is important to note that very similar results for the binding events are obtained for slightly different choices of intermediate restraining points. In addition, using a larger number of points changes very little the binding process since the approach preserves the force component along new directions, as discussed above.

C. Molecular Dynamics Simulations Details. Coordinates for LBD structures used in the simulations were obtained as follows: the structure of TRα1 bound to T3 was obtained from Prof. Robert Fletterick's homepage and is refined to a 2.0 Å resolution.[51,59] From the Protein Data Bank we obtained the structures of TRα1 and TRβ bound to KB141,[44] and of TRβ bound to GC24.[60] PDB ids and resolutions are TRα-KB141: 1NAV, 2.5 Å; TRβ-KB141: 1NAX, 2.7 Å; TRβ-GC24: 1Q4X, 2.8 Å. Structures of TRα1 and TRβ1 bound to GC1 and Triac, and for TRβ bound to T3 were obtained by Polikarpov and coworkers and are refined to 1.85, 2.1, 2.4, and 2.6 Å resolutions, respectively.[61−63] Some missing residues had to be modeled using the protocol described previously.[12] The ligands were then removed from the binding site and placed outside the protein in regions approximately related to the putative binding pathway that was going to be studied. These set of protein + ligand coordinates structures were solvated with Packmol[64] by a water shell of at least 15 Å (some 16 500 water molecules) around the LBD, containing one sodium or chloride ion for each charged protein residue or ligand. The Packmol package places all desired molecules in user-defined spatial regions avoiding overlaps between atoms of different molecules and, thus, providing an adequate initial configuration for MD simulations. Each system contained about 54 000 atoms. The energy of the system was minimized for 1000 steps of conjugate-gradient minimization, as implemented in NAMD,[55,56] keeping all the protein and ligand atoms, except the modeled ones, fixed. Three *NVT* 100 ps runs were subsequently performed for equilibration using velocity rescaling at every picosecond to a temperature of 298.15 K: first with all protein atoms fixed, except the modeled ones; and second, only the Cα atoms were kept fixed and, finally, an equilibration without any restraint was performed. We used CHARMM27[65] parameters for the protein and TIP3P parameters for water.[66] The ligand parameters were obtained by group analogy within the CHARMM27 set, as reported elsewhere.[11,12] van der Waals interactions were cutoff at 14 Å with a smooth switching function starting at 12 Å. No cutoff was used for electrostatic interactions. A time step of 2 fs was used to integrate the equations of motion. Production runs were performed in the *NVE* ensemble. Energy conservation was better than 0.5% in all simulations (the energy introduced by the external force is small relative to the total energy of the system). All simulations were performed with the NAMD simulation package.[55,56] The MP-SMD approach was implemented using the TCL scripting interface of NAMD. A steering velocity of 0.032 Å ps^{-1} and a force constant of 4.00 kcal mol^{-1} Å^{-2} were used, as in previous steered molecular dynamics investigations of ligand dissociation from NRs.[9,12] A total of 74 independent 2 ns simulations were performed and satisfactory binding events were observed in 22 of these simulations. The total simulation time was about 150 ns (including thermalization runs). The TRβ-Triac control simulation was performed with a similar protocol, but with periodic boundary conditions and PME for computing long-range electrostatic interactions. Other control simulations with other structures and ligands are found elsewhere with similar results.[11]

D. Protein Mobility. The rmsd of the Cα atoms was computed in order to investigate which residues were the most mobile during binding. The structures periodically extracted from each simulation were aligned to the native structure using a rigid body alignment algorithm[67] in order to minimize the rmsd solely for the atoms that deviate less than 4 Å from the native structure, thus emphasizing the deviation of the remaining residues. In order to identify the less mobile atoms, an iterative procedure was required. First, a rigid-body alignment considering all Cα atoms was performed. Atoms with rmsd smaller than 4 Å were then identified and the rigid-body alignment was repeated to minimize their rmsd. The procedure was repeated iteratively until the alignments converged. This way, regions that differ little from the native structure are well aligned, whereas regions of high mobility are not and can be readily identified by their corresponding deviations. Only the chain A of each PDB file has been used in the structural alignment for computing the RMSDs shown in Figure 3. All structure alignments were performed with LovoAlign.[68]

E. Justification for the Structural Models Used. There are two important drawbacks that currently prevent simulating ligand binding with the same detail and confidence as simulations of ligand dissociation from TRs. First, there is no structure of the TR LBD without ligand available. Second, even if it was available, it would be unclear whether this structure would be actually representative of the structure to which the ligand binds or important structural variations in solution precede ligand association. As already mentioned, the structures of the RAR without ligand indicate that the apo-LBD is quite different from the holo-LBD, particularly in what concerns positioning of H12.[7] Nevertheless, other apo-LBD structures are much more similar to the holo-RAR (Figure 3) than to the apo form, and in particular H12 appears closed.[23,26] The structures of the apo-ERR and apo-PPARγ receptors display deviations from the holo-TRα structure which are as small as 3.5Å (Figure 3).[23,26] Here, out of necessity, we have chosen to study ligand binding into the structure of the TR LBDs in their holo form, from which the ligand in the binding pocket is removed. The holo structures of nuclear receptors are generally more stable and less mobile than unliganded LBDs. Thus, by inducing ligand binding into the holo form of the LBD (H12 in closed lid conformation) one is presumably working away from the optimal binding conditions that are expected in an actual binding. Applied forces, energy barriers, and protein structural fluctuations during our binding simulations are, therefore, expected to be overestimated.

4. Results and Discussion

A total of 74 independent simulations of ligand binding were performed for the association of T3 and other ligands which are β-selective. Initial configurations were built for five different ligands placed outside nine different crystallographic structural models of the LBDs of TRs. This screening of ligands and structures is to provide a better sampling and independence upon initial conditions and details of ligand−protein interaction parameters rather than an analysis of the specific differences and similarities between binding of different ligands and receptor isoforms. We also keep the simulation control parameters (e.g., pulling velocity and harmonic restraining stiffness) identical to the ones used for the study of ligand dissociation[12] to render comparable results, instead of tuning them to improve successful binding rates out of the binding trials. Our goal is to obtain an overall perspective about the ligand binding process from the entire set of simulations rather than specific features for any particular system or binding trial. In 22 of these simulations, satisfactory binding trajectories were obtained, meaning that the ligand reached approximately the native position in the binding

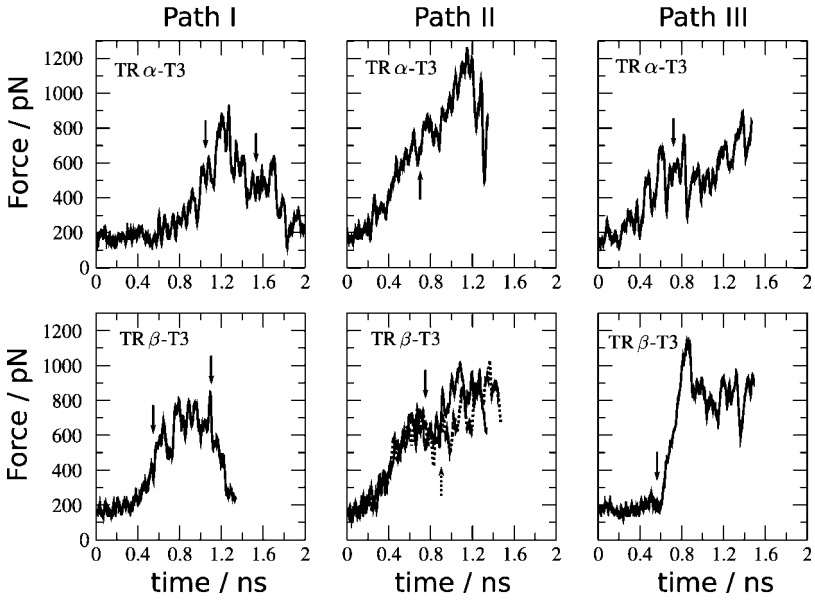

Figure 6. Force as function of simulation time for satisfactory simulations of T3 binding. For the TRβ-T3 system two independent successful binding simulations were obtained (solid and dashed). The arrows indicate the instants at which the pulling direction was changed.

TABLE 1: Maximum and Integrated Forces Binding Simulations of T3 and β-Selective Ligands[a]

simulation	path I	path II	path III
TRα-T3	902/354	1262/441	884/344
TRβ-T3	846/288	1018/378; 1029/411	1132/412
		β-Selective Ligands	
TRα-KB141	877/383	−	827/299
TRβ-KB141	815/323	1150/499	1224/244
TRβ-GC24	−	1505/242	−
TRα-Triac	831/351	904/482	1364/313
TRβ-Triac	−	1303/481	−
TRα-GC1	825/356	1274/285; 1083/275	927/287
TRβ-GC1	−	−	789/177

[a] Maximum force in pN/force integral in pN·ns.

pocket. Out of this set, six successful bindings occurred through Path I, nine through Path II, and seven through Path III. For the study of T3 binding, seven independent simulations were performed for each path, in each TR isoform. We obtained satisfactory binding in one simulation of T3 binding through Path I for each isoform, in two simulations for T3 binding through Path II to TRβ and one for TRα, and in one simulation of Path III binding for each isoform. In the remaining 52 simulations, ligand binding failed because either the ligand did not reach a satisfactory binding position in the pocket or the protein structure underwent unphysical distortions without ligand entry. This, in its own, is very suggestive of how difficult it is to induce ligand binding into NRs in simulations. In a more general perspective, the binding trajectories obtained here are qualitatively time-reversed dissociation trajectories we have obtained previously,[11,12] and clearly do not require greater protein movements (Figure S2, Supporting Information).

Figure 6 shows the driving force profiles as functions of time for each successful simulation of T3 binding. The force profiles suggest that binding through Path I seems favored because smaller barriers are involved. The maximum force barriers and time-integrated forces computed for each binding pathway (Table 1) indicate that binding through Path I requires somewhat less effort than all other pathways, except for one binding simulation through Path III into the TRα isoform. The instants at which the pulling direction was changed are indicated by arrows and the corresponding simulation snapshots are provided in Figure S1 (Supporting Information). No correlation between changes in the force and in pulling directions is observed, as expected since the technique is designed to provide smooth transitions. Figure 7 shows the force profiles as a function of simulation time for the association of several β-selective ligands. The corresponding barrier heights and time-integrated forces are shown in Table 1. Judging by the barrier heights, binding of the β-selective ligands appears to be slightly favored through Path I, similarly to T3. However, this no longer holds when considering the integrated forces since binding through Path I takes somewhat longer (~0.8 ns for Path I and 0.6 ns for Paths II and III). The force integrals for these simulations partitioned into separate pulling stages are provided in Table T1 of Supporting Information. In most cases, the approximation of the ligand to the protein surface, during the first pulling step, requires lower forces than the movement of the ligand within the protein, as expected from the specific protein−protein interactions that must be broken.

The binding simulations of the different ligands on both isoforms of the protein yields an average maximum force of 837, 1203, and 1026 pN for Paths I, II, and III, respectively, which suggests that, overall, Path I may be a preferential ligand entry route, whereas Path II seems the least favored binding pathway. But in two of the simulations the forces along Path II were similar to the ones obtained for Path I (TRα-KB141 and TRβ-GC1). If one considers the force integrals instead, then Path III appears to be the most favored and Path II the least, since the average integrated forces along Paths I, II, and III are 343, 388, and 297 pN·ns, respectively. Again, a few simulations along Path II (TRβ-GC24 and TRα-GC1) yield smaller integrated forces, similar to the ones observed for Path III. Altogether, these results indicate that a much larger number of binding simulations would be necessary to reach more conclusive results on the likelihood of individual ligand binding routes into TRs. Likewise, a quantitative assessment of the binding/unbinding free energy profiles, for instance, by means of the Jarzynski equality,[69,70] would require many runs along a given path. Nevertheless, the absence of a clear preference for a single binding pathway is strikingly different from the results obtained for ligand dissociation from TRs.[12] Previous simulations have strongly suggested that TR ligand dissociation occurs prefer-

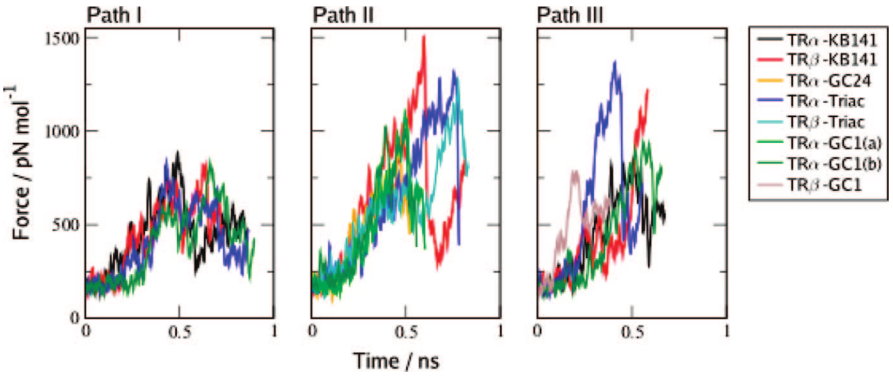

Figure 7. Force as function of simulation time for satisfactory simulations of the binding of β-selective ligands.

entially through Path III, and this is because the most important ligand−protein hydrophilic interactions are replaced by interactions between ligand and water molecules outside the LBD.[12] In addition, most of the TR ligands in that study failed to unbind through Path II, whereas binding has been observed here for all three routes, although requiring somewhat larger forces along Path II.

The applied forces involved in inducing ligand binding into TRs turned out not significantly different from the forces required to induce ligand dissociation. SMD simulations for dissociation through these paths required maximum forces ~800 pN and integrated forces smaller than 600 pN·ns for most ligands,[12] thus being roughly of the same order of the forces involved in binding (Table 1). Therefore, if the ligand dissociation paths studied previously are reasonable from the point of view of their biological significance, their closely related counterparts considered here may be also relevant pathways for ligand association. In this case, it is interesting to investigate what are the most important structural fluctuations that the LBD must undergo in order to allow for ligand association.

The prevailing model for ligand binding is based on the comparison between apo and holo crystallographic structural models.[6] As already mentioned, structures of the apo and holo RAR LBD suggest that a significant rearrangement of H12 may be involved in ligand binding and release. These structures suggest a picture in which H12 must be displaced from the body of the LBD to allow for ligand entry. While there is experimental evidence showing that the dynamics of H12 and the kinetics of ligand binding are correlated,[21] it is not clear how large are the required structural fluctuations of the LBD in order to allow ligand entry or exit. Furthermore, since several apo-LBD structures were determined which resembled the holo-RAR structure and since the corepressor binding surface requires H12 packed against the body of the receptor, the question is raised as to whether the structural fluctuations of the LBD involved in ligand binding/unbinding are as large as the ones suggested by the crystallographic models. Unbinding simulations reported by us and by others indicate that protein fluctuations much smaller than the ones associated with the apo and holo RAR structures that characterize the mousetrap model are required for ligand dissociation. In this regard, the present simulations of ligand binding suggest a novel picture for the mechanisms of ligand binding. We will show that in spite of the fact that the binding here is performed out of equilibrium, we can observe ligand association involving relatively small fluctuations of the LBD structure. This means that the view of a dynamic LBD, even if largely similar to the holo-structure, can be accepted for the apo-receptors and that ligand binding

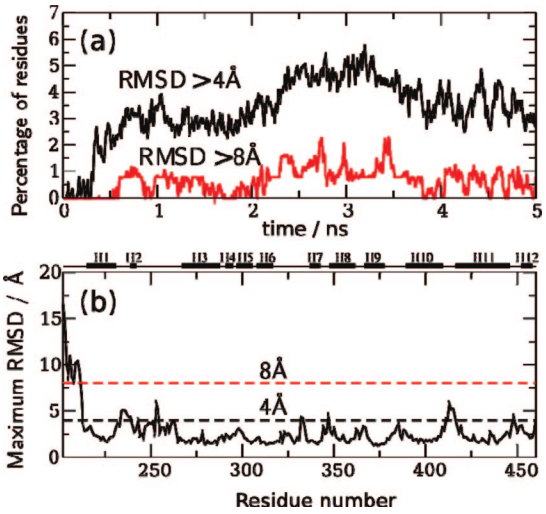

Figure 8. Molecular mobility studied in a typical control simulation: (a) percentage of residues that deviate from their native positions in more than 4 or 8 Å as function of time; (b) maximum rmsd relative to the native structure exhibited by the Cα atom of each residue during the simulation.

may be essentially a result of ligand diffusion through the receptor's surface rather than a protein-gated mechanism.

In order to measure the extent of the protein fluctuations that were required for ligand binding, we first analyzed the mobility of the structure of TRβ bound to Triac in a 5 ns control simulation (other control simulation performed with a different ligand and TR isoform has been reported elsewhere[12]). The study of the mobility of the structure in this simulation is representative of the mobility of the LBDs of TRs and is shown in Figure 8. In Figure 8a we see that in a typical equilibrium simulation, up to 5% of the Cα carbon atoms of the LBD deviate more than 4 Å from their positions in the native structure at a given time and only about 2% of the residues may deviate more than 8 Å. In Figure 8b we see that the deviations above 8 Å correspond to the structural oscillations of the highly mobile N-terminal hinge that is present in this structure and connects the LBD to the DBD.[63] Residues that deviate more than 4 Å from the native structure can be found also in the loop between H1 and H2 (the region near the β-hairpin), the loop between H2 and H3 (the Ω-loop), and other loops between some other helical motifs (H6 and H7, H10 and H11, and H11 and H12). These structural fluctuations are consistent with other control simulations and with the observed B-factors of the crystallographic structures.[51,62,63]

The key point we would like to address is how large are the structural fluctuations of the LBD involved in the ligand binding process. Most TR ligands consist of about 30 to 50 atoms, and

TABLE 2: Maximum Percentage of Residues Presenting Rmsd Larger than 4 Å Relative to the Native Structure during Binding Simulations[a]

path I	path II	path III
TRα-T3: 12.9%	TRα-T3: 42.0%	TRα-T3: 27.5%
TRβ-T3: 28.0%	TRβ-T3(1/2): 32.7/38.1%	TRβ-T3: 23.1%
TRα-KB141: 21.3%	TRα-KB141: 25.2%	TRα-KB141: 22.8%
TRβ-KB141: 11.6%	TRβ-GC24: 20.9%	**TRβ-KB141: 10.4%**
TRα-Triac: 9.4%	TRα-Triac: 23.3%	TRα-Triac: 16.8%
TRα-GC1: 8.2%	TRβ-Triac: 40.0%	**TRα-GC1: 12.4%**
	TRα-GC1(1/2): 10.1/8.2%	**TRβ-GC1: 10.0%**

[a] Simulations with the smallest fractions of residues with rmsd >4 Å are highlighted.

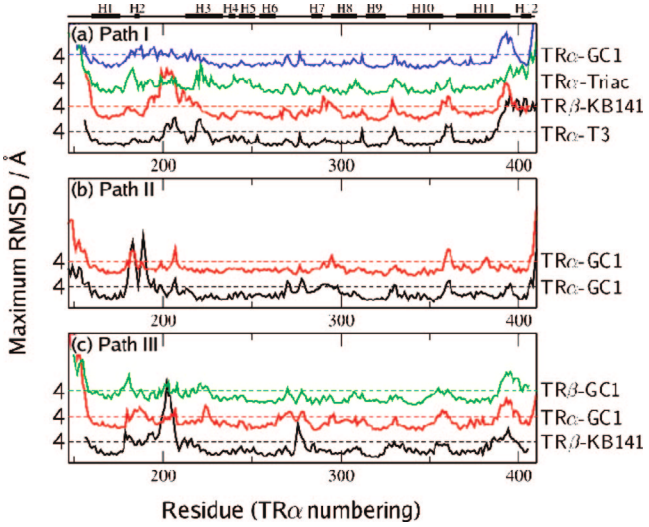

Figure 9. Maximum rmsd relative to the native structure exhibited by Cα atoms during binding simulations. Most atoms experience only small (<4 Å) deviations, indicating that only subtle structural fluctuations are required for ligand entry.

contain phenyl rings, which are fairly rigid but also flat. Here, the most extended ligand is GC24, whose (flat) molecular extension is accommodated by the LBD in a structure that is very similar to the T3 bound receptor to the point that GC24 exhibits agonist activity.[60] In 9 of the 22 simulations of ligand binding, we observed that less than ~13% of the residues underwent deviations larger than 4 Å from the native structure (highlighted simulations in Table 2). Considering that in a control (equilibrium) simulation about 6% of the residues already display mobilities of this order, this implies that only about 2−7% of the residues are required to be displaced from their native positions during ligand entry.[71] It would be interesting to compute the energetic costs involved in these motions during binding relative to the equilibrium energies. Out of the nine simulations with lowest structural fluctuations during binding, four were associated with binding through Path I, two through Path II, and three through Path III. The rmsd of the backbone carbon atoms during each of these binding simulations are depicted in Figure 9. For comparison, the rmsd deviation of the H12 from the apo- to the holo-RARα structures varies from 20 up to almost 50 Å and by itself already involves the concerted movement of the last 21 (or 9%) residues of the sequence (Figure S3, Supporting Information).

In the binding simulations through Path I that involved only small structural fluctuations of the LBD (Table 2, highlighted, and Figure 9a), there are some important movements of the N-terminal hinge and the Ω-loop, also observed in the control simulation, and of some interhelical loops. The fundamental difference from the equilibrium mobility (control simulation) lies in the larger amplitude movements exhibited by H12 and the C-terminal region of the H11 during binding. However, even these movements are quite modest and do not surpass 8 Å relative to the native structure, except for the highly mobile C-terminal residues. It is illustrative to show these protein motions directly in the LBD structure, as shown by the overlap of trajectory snapshots for one of these simulations, represented in Figure 10. Figure 10a shows that a small displacement of the H12 apart from H3 and the breaking of H3 into two helices (separated by Proline α-224/β-278 residue present in this position in TRs) are sufficient for ligand binding.

Protein motions during binding simulations through Paths II and III present similar features, but evidently in different regions of the LBD structure. The two independent TRα-GC1 simulations with smallest rmsd during binding through Path II display large mobility in the N-terminal H1 (Figure 9b). One of the simulations involved a larger displacement of the loop between H2 and H3 (Figure 9b, black curve), and both involved some displacement of the loops between H10 and H11. Further illustration of the associated protein motions during binding through Path II is depicted in Figure 10b which shows that ligand binding along the route involves some H8 bending away from H11 and the displacement of the Ω-loop (between H2 and

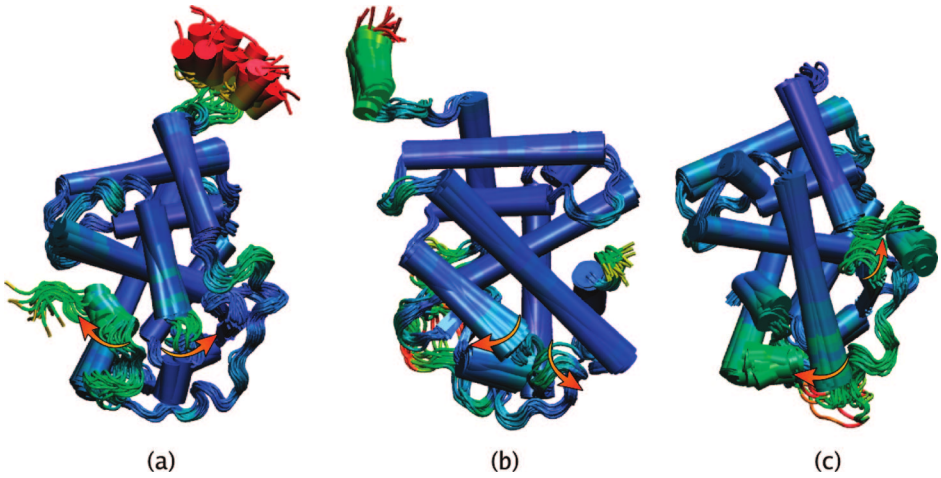

Figure 10. Illustration of the molecular movements during ligand entry into the LBD. Overlapped snapshots for simulations of ligand binding through (a) Path I (images from the TRα-Triac simulation), (b) Path II (TRα-GC1) and (c) Path III (TRβ-KB141). Structure alignment was performed according to the procedure described in section 3D.

H3). Again, these movements do not significantly distort the protein structure. The Ω-loop is naturally mobile, particularly in TRβ structures, and the bending of the H8 did not imply in any loss of secondary structure content. Therefore, binding through Path II is also possible with gentle movements of the LBD structure.

Binding through Path III involves larger movements of the loop between H1 and H2 relative to the control simulation (Figure 9c). This region is near the β-hairpin and comprises the region through which the ligand must enter in this putative binding pathway. H3 is also bent apart from the β-hairpin during binding, such that it pushes away the loop between H11 and H12 and the C-terminal region of H11. These regions display somewhat higher mobility in Path III binding simulations than in the control simulation (Figure 9c). Nevertheless, all structural rearrangements involved in binding are, again, small-amplitude motions and can be interpreted as fluctuations of the protein structure that allow for ligand entry into the binding pocket. Figure 10c shows that the displacement of H3 does not require any disruption of its secondary structure and that the major movements detected involve regions that are already mobile in TRs, such as the loop between H1 and H2, the β-hairpin, and the region between H11 and H12. Therefore, binding through Path III also does not require major protein structural rearrangements.

5. Concluding Remarks

In this work, we report the first simulation study of the mechanisms of ligand binding into the LBD of nuclear hormone receptors. The present work complements the picture of ligand recognition mechanism by nuclear receptors obtained by previous simulations of ligand dissociation performed on TRs and other NRs. For the study of the binding mechanisms we developed a generalized multipoint steered molecular dynamics approach that allows for simulating arbitrary nonlinear driving paths, which are required for proper ligand binding into the deeply buried LBD hydrophobic binding pocket. The method preserves the applied force time profile by redefining the displacement of the tagged atom at each intermediary restraining point along the driving path and can be readily applied to other complex ligand−protein or protein−protein systems in which arbitrarily shaped binding/unbinding pathways are involved. Using this approach we were able to obtain more than 20 satisfactory binding simulations in which the ligands left the solvent and reached their native positions in the binding pocket within a reasonable spatial constrain tolerance, in spite of the approximated, but structurally tighter, LBD structure used in our binding simulations.

Strikingly, the protein movements that are involved in the ligand entry processes were often quite small and conformational changes are gentle. Small protein fluctuations, not much larger than the ones observed under equilibrium control simulations, are sufficient to permit ligand entry into the LBD of thyroid hormone nuclear receptors, reaching the native ligand position. The results are robust not only because of the number of simulations and ligand variety, but also, and perhaps more importantly, because of the nature of the SMD simulations which tends to overestimate the protein distortions under applied forces, given that the pulling simulations are conducted on relatively short time scales and portrays the system out of equilibrium. Therefore, the fact that, for a significant number of simulations, small structural fluctuations are sufficient to promote proper binding indicates that this picture of ligand binding to NRs may be more general and relevant in biological contexts. Our simulations suggest that extensive conformational changes of the LBD, such as the ones inspired by the apo and holo structures of RAR (mousetrap), may not be required for ligand binding or, according to previous studies, for ligand dissociation from NRs. Therefore, the results found here combined with previous simulations of ligand dissociation provide a novel view for the process of ligand−NR binding and unbinding in which only relatively modest local structural fluctuations of a dynamic LBD may be involved. Evidently, our simulations furnish no information about the unliganded TR LBD structure and do not discard the possibility of large protein structural rearrangements being involved in the binding of ligands into NRs. In fact, it is not difficult to envisage that an open conformation of H12, for instance, would actually facilitate ligand entry through one of the pathways considered (Path I). What our simulations do suggest, however, is that unliganded LBDs can be structurally similar to holo-LBDs and yet permit ligand entry by means of modest structural fluctuations. Large conformational changes of H12 might be more important for triggering coregulators recruitment and dissociation than for ligand binding per se. The constitutive NRs activity, the conformations of the H12 required for corepressor recruitment, and the known structures of several NR apo-LBDs in closed conformation provide support to this interpretation.

Acknowledgment. We thank the Brazilian agencies FAPESP (grants 06/00182-8 to I.P. and M.S., and 06/06831-8 to L.M.) and CNPq. L.M. also thanks CAPES for financial support.

Supporting Information Available: Further details of the binding/unbinding pathways, LBD mobility from apo- and holo-RAR crystal structures, and average integrated forces during different stages of ligand binding. This material is available free of charge via the Internet at http://pubs.acs.org.

References and Notes

(1) Bain, D. L.; Heneghan, A. F.; Connaghan-Jones, K. D.; Miura, M. T. *Annu. Rev. Physiol.* **2007**, *69*, 201.
(2) Nettles, K. W.; Greene, G. L. *Annu. Rev. Physiol.* **2005**, *67*, 309.
(3) Ribeiro, R. C. J.; Kushner, P. J.; Baxter, J. D. *Annu. Rev. Med.* **2005**, *46*, 443.
(4) Weatherman, R. V.; Fletterick, R. J.; Scanlan, T. S. *Annu. Rev. Biochem.* **1999**, *68*, 559.
(5) Togashi, M.; Borngraeber, S.; Sandler, B.; Fletterick, R. J.; Webb, P.; Baxter, J. D. *J. Steroid. Biochem.* **2005**, *93*, 127.
(6) Moras, D.; Gronemeyer, H. *Curr. Opin. Cell Biol.* **1998**, *10*, 384.
(7) Egea, P. F.; Mitschler, A.; Rochel, N.; Ruff, M.; Chambon, P.; Moras, D. *EMBO J.* **2000**, *19*, 2592.
(8) Blondel, A.; Renaud, J. P.; Fischer, S.; Moras, D.; Karplus, M. *J. Mol. Biol.* **1999**, *291*, 101.
(9) Kosztin, D.; Izrailev, S.; Schulten, K. *Biophys. J.* **1999**, *76*, 188.
(10) Carlsson, P.; Burendahl, S.; Nilsson, L. *Biophys. J.* **2006**, *91*, 3151.
(11) Martínez, L.; Sonoda, M. T.; Webb, P.; Skaf, M. S.; Polikarpov, I. *Biophys. J.* **2005**, *89*, 2011.
(12) Martínez, L.; Webb, P.; Polikarpov, I.; Skaf, M. S. *J. Med. Chem.* **2006**, *49*, 23.
(13) Genest, D.; Garnier, N.; Arrault, A.; Marot, C.; Morin-Allory, L.; Genest, M. *Eur. Biophys. J.* **2008**, *37*, 369.
(14) Sonoda, M. T.; Martínez, L.; Webb, P.; Skaf, M. S.; Polikarpov, I. *Mol. Endocrinol.* **2008**, *22*, 1565.
(15) Isralewitz, B.; Baudry, J.; Gullinsgrud, J.; Kosztin, D.; Schulten, K. *J. Mol. Graph.* **2001**, *19*, 13.
(16) Bourget, W.; Ruff, M.; Chambon, P.; Gronemeyer, H.; Moras, D. *Nature* **1995**, *375*, 377.
(17) Renaud, J. P.; Rochel, N.; Ruff, M.; Vivat, V.; Chambon, P.; Gronemeyer, H.; Moras, D. *Nature* **1995**, *378*, 681.
(18) Brzozowski, A. M.; Pike, A. C.; Dauter, Z.; Hubbard, R. E.; Bonn, T.; Engström, O.; Ohman, L.; Greene, G. L.; Gustafsson, J. A.; Carlquist, M. *Nature* **1997**, *389*, 753.
(19) Tanenbaum, D. M.; Wang, Y.; Williams, S. P.; Sigler, P. B. *Proc. Natl. Acad. Sci. U.S.A.* **1998**, *95*, 5998.
(20) Celik, L.; Lund, J. D. D.; Schiott, B. *Biochemistry* **2007**, *46*, 1743.

(21) Carlson, K. E.; Tamrazi, A.; Katzenellenbogen, J. A. *Mol. Endocrinol.* **2003**, *17*, 2593.

(22) Bledsoe, R. K.; Montana, V. G.; Stanley, T. B.; Delves, C. J.; Apolito, C. J.; McKee, D. D.; Consler, T. G.; Parks, D. J.; Stewart, E. L.; Willson, T. M.; Lambert, M. H.; Moore, J. T.; Pearce, K. H.; Xu, H. E. *Cell* **2002**, *110*, 93.

(23) Nolte, R. T.; Wisely, G. B.; Westin, S.; Cobb, J. E.; Lambert, M. H.; Kurokawa, R.; Rosenfeld, M. G.; Willson, T. M.; Glass, C. K.; Milburn, M. V. *Nature* **1998**, *395*, 137.

(24) Darimont, B. D.; Wagner, R. L.; Apriletti, J. W.; Stallcup, M. R.; Kushner, P. J.; Baxter, J. D.; Fletterick, R. J.; Yamamoto, K. R. *Genes Dev.* **1998**, *12*, 3343.

(25) Shiau, A. K.; Barstad, D.; Loria, P. M.; Cheng, L.; Kushner, P. J.; Agard, D. A.; Greene, G. L. *Cell* **1998**, *95*, 927.

(26) Wang, L.; Zuercher, W. J.; Consler, T. J.; Lambert, M. H.; Miller, A. B.; Orband-Miller, L. A.; McKee, D. D.; Willson, T. M.; Nolte, R. T. *J. Biol. Chem.* **2006**, *281*, 37773.

(27) Flaig, R.; Greschik, H.; Peluso-Iltis, C.; Moras, D. *J. Biol. Chem.* **2005**, *280*, 19250.

(28) Baker, K. D.; Shewchuk, L. M.; Kozlova, T.; Makishima, M.; Hassell, A.; Wisely, B.; Caravella, J. A.; Lambert, M. H.; Reinking, J. L.; Krause, H.; Thummel, C. S.; Willson, T. M.; Mangelsdorf, T. J. *Cell* **2003**, *113*, 731.

(29) Greschik, H.; Flaig, R.; Renaud, J. P.; Moras, D. *J. Biol. Chem.* **2004**, *279*, 33639.

(30) Kallen, J.; Schlaeppi, J. M.; Bitsch, F.; Filipuzzi, I.; Schlib, A.; Riou, V.; Graham, A.; Strauss, A.; Geiser, M.; Fournier, B. *J. Biol. Chem.* **2004**, *279*, 49330.

(31) Kallenberger, B. C.; Love, J. D.; Chatterjee, V. K.; Schwabe, J. W. *Nat. Struct. Biol.* **2003**, *10*, 136.

(32) Elhaji, Y. A.; Stoica, I.; Dennis, S.; Purisima, E. O.; Trifiro, M. A. *Hum. Mol. Genet.* **2006**, *15*, 921.

(33) Frego, L.; Davidson, W. *Protein Sci.* **2006**, *15*, 722.

(34) Carlson, K. E.; Choi, I.; Gee, A.; Katzenellenbogen, B. S.; Katzenellenbogen, J. A. *Biochemistry* **1997**, *36*, 14897.

(35) Elber, R.; Karplus, M. *J. Am. Chem. Soc.* **1990**, *112*, 9161.

(36) Apriletti, J. W.; Ribeiro, R. C. J.; Wagner, R. L.; Feng, W.; Webb, P.; Kushner, P. J.; West, B. L.; Nilsson, S.; Scanlan, T. S.; Fletterick, R. J; Baxter, J. D. *Clin. Exp. Pharmacol. Physiol.* **1998**, *25*, S2–S11.

(37) González-Sancho, J. M.; García, V.; Bonilla, F.; Muñoz, A. *Cancer Lett.* **2003**, *192*, 121.

(38) Lazar, M. A. *Endocrinology* **2000**, *141*, 3055.

(39) Huber, B. R.; Desclozeaux, M.; West, B. L.; Lima, S. T. C.; Nguyen, H. T.; Apriletti, J. W.; Baxter, J. D.; Fletterick, R. J. *Mol. Endocrinol.* **2003**, *17*, 643.

(40) WebbP.; Nguyen, N.-H.; Chiellini, G.; Yoshihara, H. A. I.; Lima, s. T. C.; Apriletti, J. W.; Ribeiro, R. C. J.; Marimuthu, A.; West, B. L.; Goedec, P.; Mellstrom, K.; Nilsson, S.; Kushner, P. J.; Fletterick, R. J.; Scanlan, T. S.; Baxter, J. D. *J. Steroid Biochem. Mol. Biol.* **2003**, *83*, 59.

(41) Webb, P. *Expert Opin. Invest. Drugs* **2004**, *13*, 489.

(42) Johansson, L.; Rudling, M.; Scanlan, T. S.; Lundasen, T.; Webb, P.; Baxter, J. D.; Angelin, B.; Parini, P. *Proc. Natl. Acad. Sci. U.S.A.* **2005**, *102*, 10297.

(43) Wagner, R. L.; Huber, B. R.; Shiau, A. K.; Kelly, A.; Lima, S. T. C.; Scanlan, T. S.; Apriletti, J. W.; Baxter, J. D.; West, B. L.; Fletterick, R. J. *Mol. Endocrinol.* **2001**, *15*, 398.

(44) Ye, L.; Li, Y. L.; Mellstrom, K.; Mellin, C.; Bladh, L. G.; Koehler, K.; Garg, N.; Garcia Collazo, A. M.; Litten, C.; Husman, B.; Persson, K.; Ljunggren, J.; Grover, G.; Sleph, P. G.; George, R.; Malm, J. *J. Med. Chem.* **2003**, *46*, 1580.

(45) Hangeland, J. J.; Doweyko, A. M.; Dejneka, T.; Friends, T. J.; Devasthale, P.; Mellström, M.; Sandberg, J.; Grynfarb, M.; Sack, J. S.; Einspahr, H.; Färnegardh, M.; Husman, B.; Ljunggren, J.; Koehler, J.; Sheppard, C.; Malm, J.; Ryono, D. E. *Bioorg. Med. Chem. Lett.* **2004**, *14*, 3549.

(46) Hedfors, A.; Appelqvist, T.; Carlsson, B.; Bladh, L. G.; Litten, C.; Agback, P.; Grynfarb, M.; Koehler, K. F.; Malm, J. *J. Med. Chem.* **2005**, *48*, 3114.

(47) Li, Y. L.; Koehler, K. F.; Mellström, K.; Garg, N.; Garcia Collazo, A. M.; Färnegard, M.; Gynfarb, M.; Husman, B.; Sandberg, J.; Malm, J. *Bioorg. Med. Chem. Lett.* **2006**, *16*, 884.

(48) Garcia Collazo, A. M.; Koehler, K. F.; Garg, N.; Färnegardh, M.; Husman, B.; Ye, L.; Ljunggren, J.; Mellström, K.; Sandberg, J.; Grynfarb, M.; Ahola, H.; Malm, J. *Bioorg. Med. Chem. Lett.* **2006**, *16*, 1240.

(49) Koehler, K. F.; Gordon, S.; Brandt, P.; Carlsson, B.; Backsbro-Saeidi, A.; Apelqvist, T.; Agback, P.; Grover, G. J.; Nelson, W.; Grynfarb, M.; Färnegardh, M.; Rehnmark, S.; Malm, J. *J. Med. Chem.* **2006**, *49*, 6635.

(50) Dow, R. L.; Schnelier, S. R.; Paight, E. S.; Hank, R. F.; Chiang, P.; Cornelius, P.; Lee, E.; Newsome, W. P.; Swick, A. G.; Spitzer, J.; Hargrove, D. M.; Patterson, T. A.; Pandit, J.; Chrunyk, B. A.; LeMotte, P. K.; Danley, D. E.; Rosner, M. H.; Ammirati, M. J.; Simons, S. P.; Schulte, G. K.; Tate, B. F.; DaSilva-Jardine, P. *Bioorg. Med. Chem. Lett.* **2003**, *13*, 379.

(51) Wagner, R. L.; Aprietti, J. W.; McGrath, M. E.; West, B. L.; Baxter, J. D.; Fletterick, R. J. *Nature* **1995**, *378*, 690.

(52) Izrailev, S.; Crofts, A. R.; Berry, E. A.; Schulten, K. *Biophys. J.* **1999**, *77*, 1753.

(53) Niu, C.; Xu, Y.; Xu, Y.; Luo, X.; Duan, W.; Silman, I.; Sussman, J. L.; Zhu, W.; Chen, K.; Shen, J.; Jiang, H. J. *Phys. Chem. B* **2005**, *109*, 23730.

(54) Liu, X.; Xu, Y.; Wang, X.; Barrantes, F. J.; Jiang, H. *J. Phys. Chem. B* **2008**, *112*, 4087.

(55) Kalé, L.; Skeel, R.; Bhandarkar, M.; Brunner, R.; Gursoy, A.; Krawetz, N.; Phillips, J.; Shinozaki, A.; Varadarajan, K.; Schulten, K. *J. Comput. Phys.* **1999**, *151*, 283.

(56) Phillips, J. C.; Braun, R.; Wang, W.; Gumbart, J.; Tajkhorshid, E.; Villa, E.; Chipot, C.; Skeel, R. D.; Kale, L.; Schulten, K. *J. Comput. Chem.* **2005**, *26*, 1781.

(57) Humphrey, W.; Dalke, A.; Schulten, K. *J. Mol. Graph.* **1996**, *14*, 33.

(58) Stone, J. E.; Gullingsrud, J.; Schulten, K.; Grayson, P. A System for Interactive Molecular Dynamics Simulations. In *ACM Symposium on Interactive 3D Graphics*; Hughes, J. F., Sequin, C. H., Eds.; ACM SIGGRAPH: New York, 2001.

(59) Fletterick, R. J. http://www.msg.ucsf.edu/flett/. Technical report, UCSF, 2002.

(60) Borngraeber, S.; Budny, M. J.; Chiellini, G.; Lima, S. T. C; Togashi, M.; Webb, P.; Baxter, J. D.; Scanlan, T. S.; Fletterick, R. J. *Proc. Natl. Acad. Sci. U.S.A.* **2003**, *100*, 15358.

(61) Bleicher, L.; Aparicio, R.; Nunes, F. M.; Martínez, L.; Dias, S. M. G.; Figueira, A. C.M.; Santos, M. A. M.; Venturelli, W. H.; Silva, R.; Donate, P. M.; Neves, F. A. R.; Simeoni, L. A.; Baxter, J. D.; Webb, P.; Skaf, M. S.; Polikarpov, I. *BMC Struct. Biol.* **2008**, *8*, 8.

(62) Nunes, F. M.; Aparicio, R.; Santos, M. A. M.; Portugal, R. V.; Dias, S. M. G.; Neves, F. A. R.; Simeoni, L. A.; Webb, P.; Baxter, J. D.; Polikarpov, I. *Act. Crystallogr. D* **2004**, *10*, 1867.

(63) Nascimento, A. S.; Dias, S. M.; Nunes, F. M.; Ambrósio, A. L. B.; Aparicio, R.; Bleicher, L.; Figueira, A. C. M.; Neto, M. D.; Santos, M. A. M.; Fischer, H.; Togashi, M.; Craievich, A. F.; Garratt, R. C.; Baxter, J. D.; Webb, P.; Polikarpov, I. *J. Mol. Biol.* **2006**, *360*, 586.

(64) Martínez, J. M.; Martínez, L. *J. Comput. Chem.* **2003**, *24*, 819. Available for free download at http://www.ime.unicamp.br/~martinez/packmol.

(65) MacKerell, A. D.; Bashford, D.; Bellott, M.; Dunbrack, R. L.; Evanseck, J. D.; Field, M. J.; Fischer, S.; Gao, J.; Guo, H.; Ha, S.; Joseph-McCarthy, D.; Kuchnir, L.; Kuczera, K.; Lau, F. T. K.; Mattos, C.; Michnick, S.; Ngo, T.; Nguyen, D. T.; Prodhom, B.; Reiher, W. E.; Roux, B.; Schlenkrich, M.; Smith, J. C.; Stote, R.; Straub, J.; Watanabe, M.; Wiorkiewicz-Kuczera, J.; Yin, D.; Karplus, M. *J. Phys. Chem. B* **1998**, *102*, 3586.

(66) Jorgensen, W. L.; Chandrasekhar, J.; Madura, J. D.; Impey, R. W.; Klein, M. L. *J. Chem. Phys.* **1983**, *79*, 926.

(67) Kearsley, S. K. *Acta Crystallogr. A* **1989**, *45*, 208.

(68) Martínez, L.; Andreani, R.; Martínez, J. M. *BMC Bioinformatics* **2007**, *8*, 306.

(69) Jarzynski, C. *Phys. Rev. Lett.* **1997**, *78*, 2690.

(70) Park, S.; Khalili-Araghi, F.; Tajkhorshid, E.; Schulten, K. *J. Chem. Phys.* **2003**, *119*, 3559.

(71) Percentages in Table 2 varies from ~8% to 13%. Considering that ~6% residues with rmsd > 4 Å correspond to normal fluctuations of the LDB, one is left an excess of 2−7% residues that must displace for ligand binding.

JP803403C